Quantum Monte Carlo Calculations of Light Nuclei

R. B. Wiringa*)

Physics Division, Argonne National Laboratory, Argonne, IL 60439, U.S.A.

(Received)

Accurate quantum Monte Carlo calculations of ground and low-lying excited states of light p-shell nuclei have been made for realistic nuclear forces. These include two-nucleon potentials that reproduce nucleon-nucleon scattering data and meson-exchange three-nucleon potentials constrained to reproduce the binding energies of s-shell nuclei. At present, results for more than 40 different $(J^\pi;T)$ states in $A \leq 10$ nuclei, plus isobaric analogs, have been obtained, with an excellent reproduction of the experimental energy spectrum. These microscopic calculations show that nuclear structure, including both single-particle and clustering aspects, can be explained starting from elementary two- and three-nucleon interactions.

§1. Introduction

A major goal of nuclear physics is to understand the stability, structure, and reactions of nuclei as a consequence of the interactions between individual nucleons. Tremendous progress has been made in the past decade in the characterization of nuclear forces, with sophisticated new partial-wave analyses [1] and a number of two-nucleon potential models that fit NN data with a χ^2/datum near unity [2)-4)]. Improved three-nucleon potentials have also been constructed using pion-exchange and chiral symmetry inputs [5),6)]. Concurrently, several essentially exact methods have been developed for the study of few-nucleon systems with such realistic two- and three-nucleon interactions [7),8)]. Quantum Monte Carlo (QMC) methods are now making the light p-shell nuclei accessible at the same level of accuracy [9)-13)]. This is opening new possibilities to test our NN force models in P-waves and models of NNN forces in $T = \frac{3}{2}$ states.

The QMC calculations have now been performed for more than 40 ground or low-lying excited states, plus isobaric analogs, in nuclei with $A \leq 10$. These calculations employ the Argonne v_{18} (AV18) two-nucleon potential [3] alone or with one of several three-nucleon potentials, including the Urbana IX (UIX) model [9] and new Illinois (IL1-IL5) models [6]. The first step is a variational Monte Carlo (VMC) calculation in which a trial function, $\Psi_T(J^\pi;T)$, is constructed using products of two- and three-body correlation operators acting on a fully antisymmetrized set of one-body basis states coupled to the specified quantum numbers. Metropolis Monte Carlo integration is used to evaluate $\langle\Psi_T|H|\Psi_T\rangle$ and diagonalize in the one-body basis, giving an upper bound to the specific state. This optimized Ψ_T is then used as input to the Green's function Monte Carlo (GFMC) algorithm, which projects out excited state contamination in the trial function by the Euclidean propagation $\Psi(\tau) = \exp[-(H-E_0)\tau]\Psi_T$. In the limit $\tau \to \infty$, this yields the exact Ψ_0. In practice

*) E-mail address: wiringa@anl.gov

typeset using $\mathcal{PTP}$TEX.sty <ver.1.0>

propagation to $\tau \approx 0.1$ MeV^{-1} gives a significantly improved upper bound which we estimate to be within 1-2% of the exact binding energy for a given Hamiltonian.

GFMC calculations using the AV18/IL2 Hamiltonian reproduce 27 stable or narrow ($\Gamma \leq 200$ keV) natural-parity states in $A \leq 10$ nuclei that are experimentally well known with an average rms deviation of just 500 keV[6),13)]. Many additional wide or unobserved states have been evaluated. Energy differences between isobaric analog states have been computed to study the charge-independence-breaking of the strong and electromagnetic forces. Density distributions and electromagnetic moments are also calculated. The VMC trial functions have been used in a number of initial calculations of form factors, momentum distributions, transition amplitudes and astrophysically interesting radiative capture reactions[14)-18)].

§2. Hamiltonian

The Hamiltonian includes nonrelativistic one-body kinetic energy, the AV18 *NN* potential[3)] and either the UIX[9)] or one of the new Illinois[6)] *NNN* potentials:

$$H = \sum_i K_i + \sum_{i<j} v_{ij} + \sum_{i<j<k} V_{ijk} \ . \tag{2·1}$$

The kinetic energy operator is predominantly charge-independent (CI), but has a small charge-symmetry-breaking (CSB) component due to the difference between proton and neutron masses. The AV18 is one of the modern *NN* potentials that fit *pp* and *np* scattering data up to $E_{lab} = 350$ MeV with a χ^2/datum ≈ 1. It is given by a sum of electromagnetic, one-pion-exchange, and short-range phenomenological parts:

$$v_{ij} = v_{ij}^{\gamma} + v_{ij}^{\pi} + v_{ij}^{R} \ . \tag{2·2}$$

The electromagnetic terms include one- and two-photon-exchange Coulomb interaction, vacuum polarization, Darwin-Foldy, and magnetic moment terms, all with appropriate proton and neutron form factors. The one-pion-exchange part of the potential includes both the usual CI terms and the small charge-dependent (CD) terms due to the difference in neutral and charged pion masses. The shorter-range part has about 40 parameters which are adjusted to fit the *pp* and *np* scattering data, the deuteron binding energy, and also the *nn* scattering length.

The one-pion-exchange and the remaining phenomenological part of the potential can be written as a sum of eighteen operators,

$$v_{ij}^{\pi} + v_{ij}^{R} = \sum_{p=1,18} v_p(r_{ij}) O_{ij}^{p} \ . \tag{2·3}$$

The first fourteen CI operators are

$$O_{ij}^{p=1,14} = [1, \sigma_i \cdot \sigma_j, S_{ij}, \mathbf{L}\cdot\mathbf{S}, \mathbf{L}^2, \mathbf{L}^2 \sigma_i \cdot \sigma_j, (\mathbf{L}\cdot\mathbf{S})^2] \otimes [1, \tau_i \cdot \tau_j] \ , \tag{2·4}$$

while the last four,

$$O_{ij}^{p=15,18} = [1, \sigma_i \cdot \sigma_j, S_{ij}] \otimes T_{ij}, \ \tau_{zi} + \tau_{zj} \ , \tag{2·5}$$

are the strong interaction CD and CSB terms.

The three-nucleon potentials from the Urbana series of models [19] contain a long-range two-pion-exchange P-wave term and a short-range phenomenological piece:

$$V_{ijk}^{U} = V_{ijk}^{2\pi,P} + V_{ijk}^{R} \ . \tag{2·6}$$

The UIX model has the strengths of these two terms adjusted to reproduce the binding energy of ^{3}H (in GFMC calculations) and to give a reasonable saturation density in nuclear matter (in variational chain summation calculations) when used with AV18. The Illinois models add a two-pion-exchange S-wave term and a three-pion-ring term:

$$V_{ijk}^{IL} = V_{ijk}^{2\pi,P} + V_{ijk}^{2\pi,S} + V_{ijk}^{3\pi,\Delta R} + V_{ijk}^{R} \ . \tag{2·7}$$

The two-pion-exchange S-wave term is required by chiral symmetry, but is much smaller than the P-wave term. The three-pion-ring term is also smaller but it has a distinctly different isospin dependence, which is crucial for fitting light p-shell energy levels [6]. The operator structure and radial forms are taken from standard meson-exchange theory, but the overall strengths of the four terms, and one cutoff factor in the radial dependence, are adjusted to obtain best fits to the energies of 17 narrow states in $A \leq 8$ nuclei. In practice, at most three parameters at a time can be uniquely determined from the energy calculations, so a series of five different models has been constructed in which different subsets of the parameters are fixed by external considerations, and then the remaining ones are fit.

The CD and CSB terms in H are fairly weak, so we can treat them conveniently as a first-order perturbation and use a wave function of good isospin. Also, direct GFMC calculations with the spin-dependent terms that involve the square of the orbital angular momentum operator can have large statistical fluctuations, so it is useful to define [10] a simpler isoscalar interaction, AV8$'$, which contains only the eight operators $[1, \sigma_{\mathbf{i}} \cdot \sigma_{\mathbf{j}}, S_{ij}, \mathbf{L} \cdot \mathbf{S}] \otimes [1, \tau_{\mathbf{i}} \cdot \tau_{\mathbf{j}}]$. These eight operators are chosen such that AV8$'$ reproduces the CI part of the full AV18 interaction in all S and P waves and the deuteron. The AV8$'$ interaction was recently used in a benchmark test of seven different many-body methods for solving the four-nucleon bound state, with excellent agreement between the different calculations [8].

§3. Quantum Monte Carlo

The VMC calculation begins with the construction of a trial function, $\Psi_T(J^\pi; T)$, with embedded variational parameters. We evaluate the expectation value,

$$E_T = \frac{\langle \Psi_T | H | \Psi_T \rangle}{\langle \Psi_T | \Psi_T \rangle} \geq E_0 \ , \tag{3·1}$$

using Metropolis Monte Carlo integration, and vary the parameters in Ψ_T to minimize the variational upper bound. Our most efficient trial function has the form

$$|\Psi_T\rangle = \mathcal{S} \prod_{i<j} \left(1 + U_{ij} + \sum_{k \neq i,j} \tilde{U}_{ij;k}^{TNI} \right) |\Psi_J\rangle \ . \tag{3·2}$$

The Jastrow wave function, Ψ_J, is fully antisymmetric and has the $(J^\pi;T)$ quantum numbers of the state of interest. For the s-shell nuclei we use the simple form

$$|\Psi_J\rangle = \left[\prod_{i<j<k} f^c_{ijk}\right]\left[\prod_{i<j} f_c(r_{ij})\right]|\Phi_A(JMTT_3)\rangle \ . \tag{3·3}$$

Here $f_c(r_{ij})$ and f^c_{ijk} are central two- and three-body correlation functions and Φ_A is a Slater determinant in spin-isospin space, e.g.,

$$|\Phi_4(0000)\rangle = \mathcal{A}|p\uparrow p\downarrow n\uparrow n\downarrow\rangle \ . \tag{3·4}$$

The U_{ij} and $\tilde{U}^{TNI}_{ij;k}$ in Eq.(3·2) are noncommuting two- and three-nucleon correlation operators, and $\mathcal{S}$ indicates a symmetric sum over all possible orders of these operators. The U_{ij} includes spin, isospin, and tensor terms:

$$U_{ij} = \sum_{p=2,6} u_p(r_{ij})O^p_{ij} \ , \tag{3·5}$$

where the O^p_{ij} are the same operators that appear in the NN potential. The $f_c(r)$ and $u_p(r)$ functions are generated by the solution of a set of coupled differential equations with variational parameters [20]. The $\tilde{U}^{TNI}_{ij;k}$ has the spin-isospin structure of the dominant parts of the NNN interaction as suggested by perturbation theory.

The optimal U_{ij} and $\tilde{U}^{TNI}_{ij;k}$ do not change significantly from nucleus to nucleus, but Ψ_J does. For the p-shell nuclei, Ψ_J includes a one-body part that consists of 4 nucleons in an α-like core and $(A-4)$ nucleons in p-shell orbitals. We use LS coupling to obtain the desired JM value, as suggested by standard shell-model studies [22]. We also need to sum over different spatial symmetries $[n]$ of the angular momentum coupling of the p-shell nucleons [23]. The one-body parts are multiplied by products of central pair and triplet correlation functions, which depend upon the shells (s or p) occupied by the particles and on the $LS[n]$ coupling:

$$\begin{aligned}|\Psi_J\rangle = \mathcal{A}\{ &\prod_{i<j<k} f^c_{ijk} \prod_{i<j\le 4} f_{ss}(r_{ij}) \prod_{k\le 4<l\le A} f_{sp}(r_{kl}) \\ &\sum_{LS[n]}\left(\beta_{LS[n]} \prod_{4<l<m\le A} f^{LS[n]}_{pp}(r_{lm})|\Phi_A(LS[n]JMTT_3)_{1234:5\ldots A}\rangle\right)\}\end{aligned} \tag{3·6}$$

The operator $\mathcal{A}$ indicates an antisymmetric sum over all possible partitions into 4 s-shell and $(A-4)$ p-shell particles. The pair correlation for both particles within the s-shell, f_{ss}, is set to the f_c of the α-particle. The f_{sp} is similar to f_{ss} at short range, but with a long-range tail going to a constant ≈ 1 (which allows the wave function to develop cluster structure), while the $f^{LS[n]}_{pp}$ can depend on the particular single-particle channel.

The $LS[n]$ components of the single-particle wave function are given by:

$$\begin{aligned}|\Phi_A(LS[n]JMTT_3)_{1234:5\ldots A}\rangle = |\Phi_4(0000)_{1234}\rangle \prod_{4<l\le A} \phi^{LS[n]}_p(R_{\alpha l}) \\ \left\{[\prod_{4<l\le A} Y_{1m_l}(\Omega_{\alpha l})]_{LM_{L[n]}} \times [\prod_{4<l\le A} \chi_l(\tfrac{1}{2}m_s)]_{SM_S}\right\}_{JM} \times [\prod_{4<l\le A} \nu_l(\tfrac{1}{2}t_3)]_{TT_3}\rangle \ .\end{aligned} \tag{3·7}$$

The $\phi_p^{LS}(R_{\alpha l})$ are p-wave solutions of a particle in an effective α-N potential that has Woods-Saxon and Coulomb parts. They are functions of the distance between the center of mass of the α core and nucleon l, and may vary with $LS[n]$. The wave function is translationally invariant, so there is no spurious center of mass motion. A diagonalization is carried out in the one-body basis to find the optimal values of the $\beta_{LS[n]}$ for a given $(J^\pi;T)$ state.

The trial function, Eq.(3·2), has the advantage of being efficient to evaluate while including the bulk of the correlation effects. A more sophisticated variational function can be constructed by including two-body spin-orbit correlations and additional three-body correlations[20),21)], but the time to compute these extra terms is significant, while the gain in the variational energy is relatively small.

The wave function at a given spatial configuration $\mathbf{R} = \mathbf{r}_1, \mathbf{r}_2, ...\mathbf{r}_A$ can be represented by a vector of $2^A \times I(A,T)$ complex coefficients in spin and isospin space[10)]. For the nuclei considered here, this leads to vectors ranging in length from 16 for ^{3}H to 92,160 for ^{10}Be, although a savings of a factor of two is possible in even-A nuclei by computing in the $M = 0$ substates. The spin, isospin, and tensor operators $O_{ij}^{p=2,6}$ contained in the Hamiltonian and other operators of interest are sparse matrices in this basis.

The GFMC method[24),25)] projects out the exact lowest-energy state, Ψ_0, for a given set of quantum numbers, using $\Psi_0 = \lim_{\tau\to\infty} \exp[-(H-E_0)\tau]\Psi_T$, where Ψ_T is the optimized trial function from the VMC calculation. If the maximum τ is large enough, the eigenvalue E_0 is calculated exactly while other expectation values are generally calculated neglecting terms of order $|\Psi_0 - \Psi_T|^2$ and higher[10)]. In contrast, the error in the variational energy is of order $|\Psi_0 - \Psi_T|^2$, and other expectation values calculated with Ψ_T have errors of order $|\Psi_0 - \Psi_T|$.

We define the propagated wave function $\Psi(\tau)$

$$\Psi(\tau) = e^{-(H-E_0)\tau}\Psi_T = \left[e^{-(H-E_0)\triangle\tau}\right]^n \Psi_T = G^n \Psi_T \ , \qquad (3\cdot8)$$

where we have introduced a small time step, $\tau = n\triangle\tau$. The G is calculated with leading errors of order $(\triangle\tau)^3$. Omitting spin-isospin indices for brevity, $\Psi(\mathbf{R}_n,\tau)$ is given by

$$\Psi(\mathbf{R}_n,\tau) = \int G(\mathbf{R}_n,\mathbf{R}_{n-1})\cdots G(\mathbf{R}_1,\mathbf{R}_0)\Psi_T(\mathbf{R}_0)d\mathbf{R}_{n-1}\cdots d\mathbf{R}_1 d\mathbf{R}_0 \ . \qquad (3\cdot9)$$

The short-time propagator is constructed with the exact two-body propagator and additional terms coming from the three-body interaction.

Quantities of interest are evaluated in terms of a "mixed" expectation value between Ψ_T and $\Psi(\tau)$:

$$\langle O\rangle_{\text{Mixed}} = \frac{\langle\Psi_T|O|\Psi(\tau)\rangle}{\langle\Psi_T|\Psi(\tau)\rangle} \ , \qquad (3\cdot10)$$

where the integration over different paths in Eq.(3·9) is carried out stochastically. The desired expectation values would, of course, have $\Psi(\tau)$ on both sides; by writing $\Psi(\tau) = \Psi_T + \delta\Psi(\tau)$ and neglecting terms of order $[\delta\Psi(\tau)]^2$, we obtain the expression

$$\langle O(\tau)\rangle = \frac{\langle\Psi(\tau)|O|\Psi(\tau)\rangle}{\langle\Psi(\tau)|\Psi(\tau)\rangle} \approx \langle O(\tau)\rangle_{\text{Mixed}} + [\langle O(\tau)\rangle_{\text{Mixed}} - \langle O\rangle_T] \ , \quad (3\cdot11)$$

where $\langle O\rangle_T$ is the variational expectation value. A special case is the expectation value of the Hamiltonian. The $\langle H(\tau)\rangle_{\rm Mixed}$ can be re-expressed as

$$\langle H(\tau)\rangle_{\rm Mixed} = \frac{\langle \Psi_T|e^{-(H-E_0)\tau/2}He^{-(H-E_0)\tau/2}|\Psi_T\rangle}{\langle \Psi_T|e^{-(H-E_0)\tau/2}e^{-(H-E_0)\tau/2}|\Psi_T\rangle} \geq E_0 \ , \qquad (3\cdot12)$$

since the propagator $\exp[-(H-E_0)\tau]$ commutes with the Hamiltonian. Thus $\langle H(\tau)\rangle_{\rm Mixed}$ approaches E_0 in the limit $\tau\to\infty$, and the expectation value obeys the variational principle for all τ.

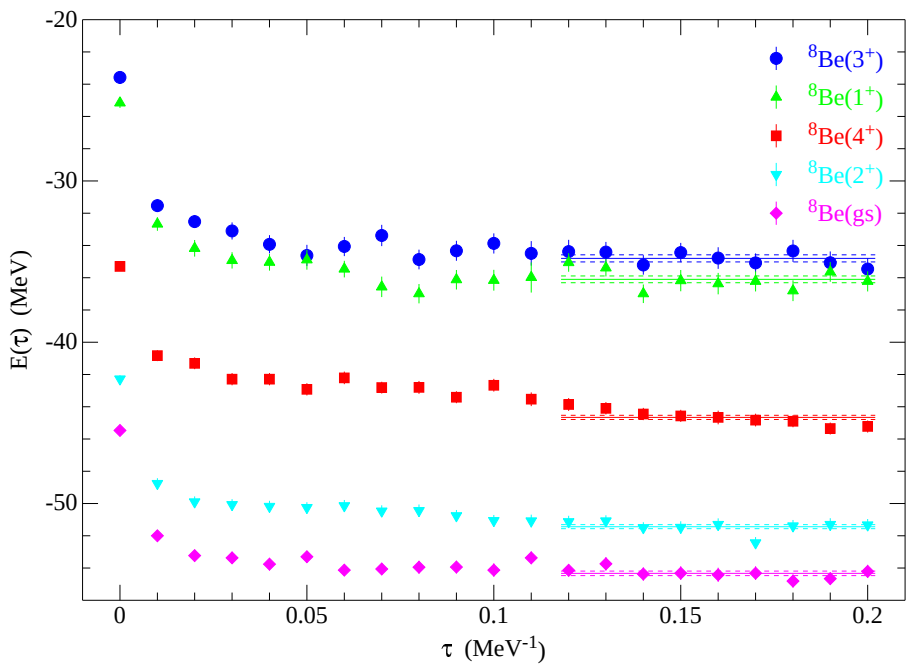

Fig. 1. GFMC $E(\tau)$ for states of ^{8}Be

As mentioned above, to reduce statistical noise, the GFMC propagation is actually made with a simplified Hamiltonian H' that includes the CI kinetic energy operator, the AV8$'$ NN interaction including isoscalar Coulomb, and a slightly altered V'_{ijk}, adjusted such that $\langle H'\rangle \approx \langle H\rangle$. Consequently, the upper bound property applies to $\langle H'(\tau)\rangle$, and $\langle H-H'\rangle$ is be evaluated perturbatively. The GFMC algorithm also suffers from a "fermion sign problem", which arises from the stochastic evaluation of the matrix elements in Eq.(3·10). The $G(\mathbf{R}_i,\mathbf{R}_{i-1})$ is a local operator and can mix in the boson solution, which has a (much) lower energy and thus is exponentially amplified in subsequent propagations. In the final integration with the antisymmetric Ψ_T, the desired fermionic part is projected out, but in the presence of statistical errors that grow exponentially with τ. Because the number of pairs that can be exchanged grows with A, the sign problem also grows exponentially with increasing A, making convergence in τ difficult for $A\geq 8$. A "constrained path" approximation has been developed [11] to remedy this problem by discarding configurations that, in future generations, will contribute only noise to expectation

values. Tests of the constrained path algorithm indicate that it gives results that are consistent with unconstrained propagation, within statistical errors.

Figure 1 shows the progress with increasing τ of typical constrained GFMC calculations, in this case for various states of ^{8}Be. The values shown at $\tau = 0$ are the VMC values using Ψ_T. The GFMC very rapidly makes a large improvement on these energies; by $\tau = 0.01$ MeV^{-1} (20 steps with $\Delta\tau = 0.0005$ MeV^{-1}), the Ψ_T energies have been reduced by 6.5 to 8 MeV. This rapid improvement corresponds to the removal of small admixtures of states with excitation energies ~ 1 GeV from Ψ_T. The standard deviation, computed using block averaging, of all of the individual energies for these τ values is used to compute the corresponding statistical error. The solid lines in Fig. 1 show the averages over that last several τ values and the dashed lines show the statistical uncertainty.

§4. Energy Results

The GFMC results for $A \leq 10$ nuclei are compared with experiment in Fig.2 for two Hamiltonians, AV18 alone and AV18/IL2. It is apparent that AV18 alone significantly underbinds these nuclei. The ordering of states is correct up to ^{10}B, but there the ground state is incorrectly predicted to be a 1^+ state. Also, the splittings between excited states that are spin-orbit partners is too small. The AV18/UIX Hamiltonian, which is not shown, does a much better job than AV18 alone, but still systematically underbinds, particularly as A or T increases, and also incorrectly predicts a 1^+ ground state for ^{10}B. However, the AV18/IL2 Hamiltonian gives a very good reproduction of these nuclei, including both absolute binding energies and spin-orbit splittings. While the IL2 *NNN* potential was adjusted to give a good fit up to $A = 8$, it continues to do an excellent job in $A = 9, 10$ nuclei. In particular, it correctly produces a 3^+ ground state in ^{10}B, as do the other new Illinois models IL3 and IL4.

Table I. Contributions to energy in GFMC calculations of AV18/IL2

$^AZ(J^\pi;T)$	^{3}H($\frac{1}{2}^+$)	^{4}He(0^+)	^{6}Li(1^+)	^{7}Li($\frac{3}{2}^-$)	^{8}Be(0^+)	^{9}Be($\frac{3}{2}^-$)	^{10}B(3^+)
E (expt)	–8.48	–28.30	–31.99	–39.24	–56.50	–58.16	–64.75
$\langle H\rangle$	–8.43(1)	–28.37(3)	–32.3(1)	–39.6(2)	–56.6(4)	–58.2(5)	–65.4(7)
$\langle K_i\rangle$	51.3(2)	115(1)	160(2)	199(3)	256(4)	285(4)	342(4)
$\langle v_{ij}\rangle$	–58.6(2)	–136(1)	–187(2)	–232(3)	–303(3)	–336(4)	–398(3)
$\langle v_{ij}^\gamma\rangle$	0.04	0.86	1.73(1)	1.80(1)	3.32(1)	3.44(1)	5.54(1)
$\langle v_{ij}^\pi\rangle$	–45	–105(1)	–150(1)	–178(2)	–234(2)	–256(2)	–305(2)
$\langle v_{ij}^R\rangle$	–14	–32(1)	–39(1)	–56(2)	–72(2)	–84(4)	–98(4)
$\langle V_{ijk}\rangle$	–1.5	–8.4(1)	–11.1(3)	–14.5(4)	–21.0(1)	–24.1(8)	–35.6(8)
$\langle V_{ijk}^{2\pi}\rangle$	–3.0	-16.3(1)	–19.8(4)	–25.6(6)	–38.5(9)	–43.8(9)	–57.3(9)
$\langle V_{ijk}^{3\pi}\rangle$	0.18(1)	0.63(1)	–0.4(1)	–1.1(1)	–0.9(2)	–2.1(2)	–5.9(3)
$\langle V_{ijk}^R\rangle$	1.3	7.3(1)	9.1(2)	12.3(4)	18.3(6)	21.7(6)	27.6(7)

A breakdown of the contributions of the different parts of the Hamiltonian to the total energy is given in Table I for a number of the nuclear ground states. (Because these are mixed expectation values, the sum of the different components does not quite add up to $\langle H\rangle$.) The large cancellation between kinetic and *NN*

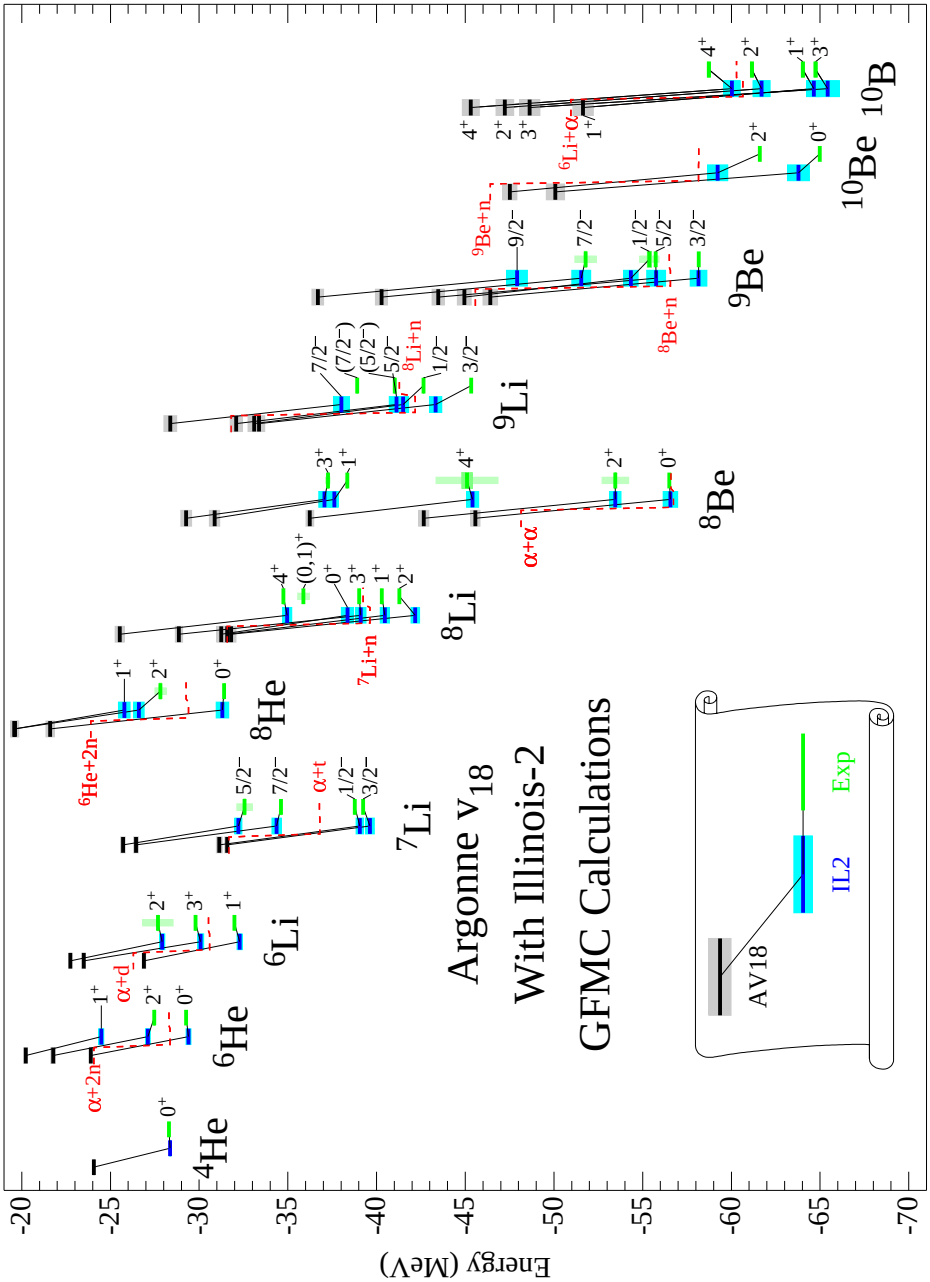

Fig. 2. GFMC energies using AV18 and AV18/IL2 compared with experiment

potential expectation values is clearly evident. The *NNN* potential expectation value is typically only 6% of the *NN* potential, but can be a third of the total binding. In principle, there will be four-nucleon and higher forces, but if these converge as rapidly as the two- and three-nucleon forces, they will be less than 1-2% of the binding energy, which is about the accuracy of the GFMC method at present. Expectation

values for different components of the *NN* and *NNN* potentials are also shown in Table I. Of particular note is the large fraction of the *NN* potential energy that is carried by the one-pion-exchange potential, v_{ij}^{π}. Similarly, the two-pion-exchange potential dominates the *NNN* potential energy, while the three-pion-exchange ring is quite small. However, this latter term becomes more important for given A as T increases.

We have also computed energy differences among isobaric analog states, which are sensitive probes of the charge-independence-breaking part of the Hamiltonian [26]. The energies for a given isomultiplet of states can be expanded as

$$E_{A,T}(T_z) = \sum_{n \leq 2T} a_n(A,T) Q_n(T,T_z) \ , \tag{4·1}$$

where $Q_0 = 1$, $Q_1 = T_z$, and $Q_2 = \frac{1}{2}(3T_z^2 - T^2)$ are isoscalar, isovector, and isotensor terms [10]. The isovector and isotensor coefficients $a_n(A,T)$, and various contributions to them, are given in Table II. These were calculated as expectation values in the $T_z = -T$ GFMC wave functions for AV18/IL2. The individual terms are: 1) the effect of the neutron-proton mass difference on the kinetic energy, K^{CSB}; 2) the proton-proton Coulomb potential, including form factors, $v_{C1}(pp)$; 3) all other electromagnetic terms such as magnetic-moment terms, $v^{\gamma,R}$; and 4) the strong-interaction contributions, v^{CSB} and v^{CD}. In general, the energy differences are explained well by the calculations. The dominant effect comes from the *pp* Coulomb energy, which is rather sensitive to the rms radius of the nucleus and thus to the overall binding energy. The additional smaller terms give important corrections that always improve the isovector energy, but sometimes overpredict the isotensor component.

Table II. GFMC isovector and isotensor energy coefficients $a_n(A,T)$ in keV, for AV18/IL2.

$a_n(A,T)$	K^{CSB}	$v_{C1}(pp)$	$v^{\gamma,R}$	v^{CSB}	v^{CD}	Total	Expt.
$a_1(3,\frac{1}{2})$	14	649(1)	29	64(0)		757(1)	764
$a_1(6,1)$	16	1091(5)	18	47(1)		1172(6)	1173
$a_1(7,\frac{1}{2})$	22	1447(6)	40	79(2)		1588(7)	1644
$a_1(8,1)$	23	1686(5)	24	76(1)		1810(6)	1770
$a_1(8,2)$	18	1528(7)	17	59(1)		1622(8)	1659
$a_1(9,\frac{1}{2})$	21	1776(9)	6	55(2)		1857(10)	1851
$a_1(9,\frac{3}{2})$	22	1824(5)	33	71(1)		1950(6)	2104
$a_1(10,1)$	22	2046(6)	29	72(2)		2169(8)	2329
$a_2(6,1)$		166(1)	19		107(13)	293(13)	223
$a_2(8,1)$		141(1)	4		–3(8)	143(8)	128
$a_2(8,2)$		136(1)	6		38(5)	180(5)	153
$a_2(9,\frac{3}{2})$		142(1)	8		43(7)	192(7)	176
$a_2(10,1)$		169(1)	13		98(25)	280(26)	241

§5. Further Remarks

In addition to the energies reported here, GFMC calculations also produce one- and two-body density distributions and magnetic and quadrupole moments [6), 10), 11)].

The VMC method has been used to study an even larger variety of phenomena, including the elastic and transition electromagnetic form factors in ^{6}Li [14], spectroscopic factors in ^{7}Li$(e,e'p)^6$He reaction [15], and transition amplitudes in pion elastic and inelastic scattering from ^{6,7}Li [16]. The low-energy radiative capture reactions ^{2}H$(\alpha,\gamma)^6$Li, ^{3}H$(\alpha,\gamma)^7$Li, and ^{3}He$(\alpha,\gamma)^7$Be, which are of interest in primordial nucleosynthesis and solar energy production, have also been studied [17),18)].

We expect to extend the QMC calculations to $A = 11, 12$ nuclei in the next few years as computer resources increase. One major challenge is the proper treatment of wide, particle-unstable states in GFMC. The VMC method has been used to study the $\alpha + n$ scattering states in ^{5}He [27], but reliable absolute energies and widths will require GFMC. We would also like to develop orthogonalization techniques so that GFMC can be used for second and higher states of given $(J^\pi; T)$. Many additional reactions and transitions in p-shell nuclei will be studied by QMC techniques.

Acknowledgments

I wish to thank S. C. Pieper, K. Varga, J. Carlson, V. R. Pandharipande, R. Schiavilla, and K. M. Nollett. Computations were made at the National Energy Research Scientific Computing Center and the Mathematics and Computer Science Division of Argonne National Laboratory. This work is supported by the U. S. Department of Energy, Nuclear Physics Division, under contract No. W-31-109-ENG-38.

References

1) V. G. J. Stoks, *et al.*, Phys. Rev. C **48** (1993), 792.
2) V. G. J. Stoks, *et al.*, Phys. Rev. C **49** (1994), 2950.
3) R. B. Wiringa, V. G. J. Stoks, and R. Schiavilla, Phys. Rev. C **51** (1995), 38.
4) R. Machleidt, F. Sammarruca, and Y. Song, Phys. Rev. C **53** (1996), R1483.
5) J. L. Friar, D. Hüber, and U. van Kolck, Phys. Rev. C **59** (1999), 53.
6) S. C. Pieper, *et al.*, Phys. Rev. C **64** (2001), 014001.
7) J. Carlson and R. Schiavilla, Rev. Mod. Phys. **70** (1998), 743.
8) H. Kamada, *et al.*, Phys. Rev. C **64** (2001), 044001.
9) B. S. Pudliner, *et al.*, Phys. Rev. Lett. **74** (1995), 4396.
10) B. S. Pudliner, *et al.*, and R. B. Wiringa, Phys. Rev. C **56** (1997), 1720.
11) R. B. Wiringa, *et al.*, Phys. Rev. C **62** (2000), 014001.
12) S. C. Pieper and R. B. Wiringa, Annu. Rev. Nucl. Part. Sci. **51** (2001), 53.
13) S. C. Pieper, K. Varga, and R. B. Wiringa, in preparation (2002).
14) R. B. Wiringa and R. Schiavilla, Phys. Rev. Lett. **81** (1998), 4317.
15) L. Lapikás, J. Wesseling, and R. B. Wiringa, Phys. Rev. Lett. **82** (1999), 4404.
16) T.-S. H. Lee and R. B. Wiringa, Phys. Rev. C **63** (2001), 014006.
17) K. M. Nollett, R. B. Wiringa, and R. Schiavilla, Phys. Rev. C **63** (2001), 024003.
18) K. M. Nollett, Phys. Rev. C **63** (2001), 054002.
19) J. Carlson, V. R. Pandharipande, and R. B. Wiringa, Nucl. Phys. **A401** (1983), 59.
20) R. B. Wiringa, Phys. Rev. C **43** (1991), 1585.
21) A. Arriaga, V. R. Pandharipande, and R. B. Wiringa, Phys. Rev. C **52** (1995), 2362.
22) S. Cohen and D. Kurath, Nucl. Phys. **73** (1965), 1.
23) A. Bohr and B. R. Mottelson, *Nuclear Structure Volume I*, App. 1C, (W. A. Benjamin, New York, 1969).
24) J. Carlson, Phys. Rev. C **36** (1987), 2026.
25) J. Carlson, Phys. Rev. C **38** (1988), 1879.
26) J. A. Nolen and J. P. Schiffer, Ann. Rev. Nucl. Sci. **19** (1969), 471.
27) J. Carlson, K. E. Schmidt, and M. Kalos, Phys. Rev. C **36** (1987), 27.